Biomacromolecules

ARTICLE

pubs.acs.org/Biomac

Early Osteogenic Differentiation of Mouse Preosteoblasts Induced by Collagen-Derived DGEA-Peptide on Nanofibrous Phage Tissue Matrices

So Young Yoo, Masae Kobayashi, Phin Peng Lee, and Seung-Wuk Lee*

Bioengineering, University of California, Berkeley, Physical Biosciences Division, Lawrence Berkeley National Laboratory, Berkeley Nanoscience and Nanoengineering Institute, Berkeley, California 94720, United States

Supporting Information

ABSTRACT: Specific biochemical and physical cues in tissue extracellular matrices play a critical role in regulating cellular growth processes and their fate. We report initial responses of bone stem cells induced by collagen-derived DGEA-peptides on nanofibrous M13 phage tissue matrices. We constructed genetically engineered M13 phage with DGEA-peptide displayed in high density on the major coat proteins and biomimetic nanofibrous tissue-like matrices in two and three dimensions. We investigated the effects of biochemical cues, specifically DGEA-peptides on preosteoblast (MC3T3) morphologies. The preosteoblasts grown on the top of the DGEA-incorporated phage matrices exhibited significant outgrown morphology with early bone cell marker protein expression. Through soluble peptide competition assays and control experiments, we verified that the observed cellular morphologies and osteogenic protein marker expression were specifically caused by the DGEA-peptides. We confirmed that the outgrown morphologies are linked with the early phase of osteogenic protein expression through mRNA quantification and bone cell protein marker expression. Additionally, we demonstrated that the phage-based tissue matrix systems could work as a good cell culture platform to investigate the specific effect of biochemical cues, which can be tuned precisely at a single amino acid level with little change in other physical and chemical properties of the environment. Our study advances the understanding of osteogenic differentiation and our phage-based tissue matrices have the potential for future bone regeneration therapy and systemic investigation of specific cellular responses to biochemical ligand stimulation.

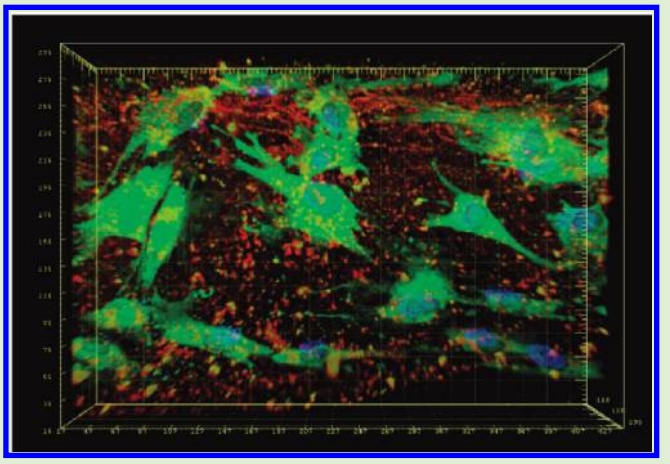

1. INTRODUCTION

Precisely designed active biomaterials with controlled structural organization are of great interest in areas of regenerative medicine, drug screening, and biosensors.[1−7] Many attempts have been made to mimic natural tissue microenvironment in vivo by using extracted extracellular matrix (ECM) or synthetic ECM-mimetic macromolecules to manipulate the ECM's biological, chemical, and mechanical properties.[8−13] The ECM is mainly composed of abundant nanometer-scale fibrous protein networks.[14−17] These nanofibrous structures provide cellular instructive signals to regulate cell−matrix interactions by presenting biochemical ligands that interact specifically with cellular integrins and other receptors to trigger cascading cellular signal transduction processes[18−20] In addition, nanometer scale topography and textures presented by individual ECM molecules play an important role in supporting and controlling desired cellular functions and morphologies. For example, collagen 300 nm in length and 1.5 nm in width[21] can form nanofibrils that extend from tens of nanometers to several micrometers in length and diameter.[22,23] Together with these ECM nanofibrous structures,[24,25] neighboring proteins, various growth factors, and chemokines provide biochemical signaling for adhesion, migration, proliferation, and differentiation.[26−28] Various ECM ligand peptide sequences have also been identified and demonstrated to regulate the cellular functions. For example, RGD peptides from fibronectin induce focal adhesion through integrin binding;[32] DGEA from collagen type I induce bone cell differentiation;[29,30] IKVAV from laminin stimulates outgrowth of neurite;[31,32] and so on. Among these peptides, RGD has been the most well-characterized to induce various cellular functions. However, collagen-derived DGEA-peptides have been relatively less investigated for their specific cellular response compared to other ECM peptides, while collagen has been mostly applied for constructing tissue engineering scaffold.[23,33−35] In particular, collagen plays a critical

Received: November 11, 2010
Revised: January 22, 2011

dx.doi.org/10.1021/bm1013475 | *Biomacromolecules* XXXX, XXX, 000–000

role in templating bone hard tissue formation in both cellular and calcification processes.[36] If a biomaterial mimics the fibrous shape and chemical structure of collagen, it might be useful for engineering bone tissue. Direct incorporation of the various biochemical ligands into synthetic biomaterials or natural materials has been used to design various tissue regenerating matrices. Although the resulting structures provide great promise to improve the quality of materials to stimulate the cells, emulating complex tissue microenvironments and precisely controlling biochemical and physical cues using conventional approaches is still highly challenging. Any modification of chemical structures requires labor-intensive chemical synthesis and the resulting chemical structures affect other important physical and mechanical parameters. A material that mimics the nanofibrous structure of the ECM and whose biochemical structure can be conveniently modified with little change in physical structure and assembly processes will be very desirable for investigating various biochemical cues and their effects on cellular growth processes.

Genetic engineering of phages provides novel opportunities to create functional nanomaterials for various applications in energy, electronics, and biomedical engineering.[37−42] In particular, phage technology has recently been greatly expanded to biomedical applications including tissue engineering, drug delivery,[43,44] and bioimaging.[45] The M13 phage is a bacterial virus with a tropism to infect only a specific bacterial strain; previous biomedical applications of phages showed that the phage is a safe material that exhibits little inflammation at a targeted brain tissue site, although its effect on other tissues have yet to be verified.[46,47] Endocytosed phages are also shown to degrade via the lysosomal pathway.[48,49]

Recently, nanofibrous structures of M13 phage have been used after chemical and genetic modification, with cell signaling peptides as novel tissue engineering matrices to direct desired cellular functions.[50−54] We demonstrated several advantages and potentials for various applications over conventional tissue engineering materials by exploiting its physical and biological structural features (such as the phage's self-assembling, self-replicating and evolving nature). First, through genetic engineering of a desired sequence insertion on the major coat protein, we could easily display high densities (1.5×10^{13} epitopes/cm^2) of signaling peptides along the surface of the nanofiber-like phage. Second, the long-rod shape and monodispersity of the phage can fabricate various self-aligned two-dimensional (2D) or three-dimensional (3D) structures from the nanometer scale to the centimeter scale. Third, the resulting structures could control physical and chemical cues to direct the growth of desired cells, including neural cells, preosteoblasts, fibroblasts, and others.[50−52] These active phage materials coupled with microfabrication techniques have demonstrated their potential as versatile biomedical platforms.[53] Therefore, phage-based tissue engineering matrices can be a good model system for investigating biochemical cues requiring a high density of functional peptides and precise tuning of the materials. Here, we report early osteogenic differentiation effects on bone stem cells induced by a collagen-derived peptide incorporated on M13 phage with a collagen-like shape. We constructed genetically engineered M13 phage with DGEA-peptide on the major coat proteins displayed in high density and biomimetic nanofibrous tissue-like matrices in two and three dimensions. Then, we investigated effects of DGEA-peptides on preosteoblast (MC3T3) morphologies in a biochemical-cue-dependent manner. Cells cultured on DGEA-incorporated phage matrices exhibited significantly outgrown morphologies with expression of early bone cell markers. Through the control experiments and soluble peptide competition assays, we confirmed that the observed cellular morphologies and osteogenic protein marker expression were caused by the DGEA-peptides. We also showed that our phage system could tune biochemical structures precisely at a single amino acid level without changing other physical and chemical environments. Our study will be useful in understanding osteogenic differentiation and our phage based tissue matrices might help develop future bone cell therapies and systemic investigation of specific cellular responses to biochemical cues.

2. EXPERIMENTAL SECTION

Cell Culture. MC3T3-E1 (ATCC CRL-2593, Manassas, VA) is a nontransformed cell line established from newborn mouse calvaria and exhibits an osteoblastic phenotype. Cells were grown in α-MEM medium supplemented with 10% FBS, 1% penicillin/streptomycin, and 1% L-glutamine. Cells were subcultured once a week using trypsin/EDTA and maintained at 37 °C in a humidified atmosphere of 5% CO_2 in air.

WST1 Proliferation Assay. The WST-1 assay (Cell Proliferation Reagent WST-1; Roche Applied Science, Basel, Switzerland) was performed as per the manufacturer's instructions. 10 μL of reagent was mixed with 0.1 mL of growth medium and added to the MC3T3-E1 cells on DGEA phage and other control matrices. The difference between the absorbance at 450 and 690 nm of the medium was read on an ELISA reader (Safire, Tecan Group Ltd., Männedorf, Switzerland).

Genetic Engineering of M13 Phage. To present peptide motifs on 2700 copies of M13 major coat protein pVIII, an inverse PCR cloning method was adapted.[55−57] To incorporate the gene sequences, polymerase chain reaction (PCR) was performed using Phusion High-Fidelity DNA Polymerase (Finnzymes, Espoo, Finland), the two primers, and an M13KE vector (Table 1 for primer sequences). The obtained product was purified on an agarose gel, eluted with spin column purification, digested with *Pst*I enzyme (New England Biolabs, Ipswich, MA), and recircularized with an overnight ligation at 16 °C with T4 DNA Ligase (New England Biolabs).[58] The ligated DNA vector was then transformed into XL10-Gold Ultracompetent bacteria cells (Stratagene, La Jolla, CA), and the amplified plasmid was verified via DNA sequencing at UC Berkeley DNA Sequencing Facility, Berkeley, CA.

Fabrication of Two-Dimensional and Phage Films and Three-Dimensional Phage Fibers. Surfaces were precoated before cell plating. Phage-coated surfaces were initially coated with poly-ornithine to allow for better adhesion of the negatively charged phage. Phage solutions in PBS (10^{12} viruses/mL) were then drop-cast on the surface and allowed to dry overnight at room temperature.[48] Three-dimensional phage nanofiber matrices were also constructed. Liquid crystalline suspensions in PBS of DGEA, RGD- and no-phage were prepared and mixed with MC3T3 cells in media to give a final concentration of ∼15 mg phage/mL. This suspension was then manually injected at a rate of approximately 0.8 ± 0.1 μL/sec directly into low melting temperature liquid agarose. The agarose cooled and solidified around the phage-cell fiber, trapping the mixture and allowing for a convenient system for cell culture maintenance and sample observation.

DGEA- and RGD-Peptide Synthesis. RGD- and DGEA-peptides were synthesized using the fluorenyl-methoxy-carbonyl (Fmoc)−solid-phage peptide synthesis method on the resin (50 μmol based on the resin substitution level). Stepwise couplings of amino acids were accomplished using a double coupling method with 5-fold excesses of amino acids, equivalent activator reagents *N*,*N*′-diisopropyl carbodiimide (DIC) and *N*-hydroxybenzotriazole (HOBt).

Competition Assays. MC3T3 cells were seeded on DGEA-phage drop-cast films at a density of $\sim 1.8 \times 10^3$ cells/cm^2 in the presence of different concentrations of soluble DGEA- or RGD-peptides synthesized

Table 1. Primer Sequences for pVIII Engineering

name	oligonucleotide primer sequence[a]	insert peptide sequence[b]
p8-DGEA	5′ATATAT**CTGCAG***ATGGTGAGGCT*GATCCCGCAAAAGCGGCC 3′	A*DGEA*DP
p8-DGDA	5′ATATAT**CTGCAG***ATGGTGATGCT*GATCCCGCAAAAGCGGCC 3′	A*DGDA*DP
p8-EGEA	5′ATATAT**CTGCAG***AGGGTGAGGCT*GATCCCGCAAAAGCGGCC 3′	A*EGEA*DP
p8-RGD	5′ ATATAT**CTGCAG***NK (NNK)*$_2$*CGTGGT GAT (NNK)*$_2$GATCCCGCAAAAGCGGCCTTTAACTCCC 3′	A*DSGRGDTE*DP [c] (A*XXXRGDXX*DP)
p8-RGE	5′ATATAT**CTGCAG***ACTCGGGACGTGGTGA AACCGAA*GATCCCGCAAAAGCGGCCTTTAACTCCC 3′	A*DSGRGETE*DP
p8-rev1376	5′ CCT**CTGCAG**CGAAAGACAGCATCGG 3′	

[a] For primer oligonucleotide sequences the restriction sites are shown in **bold**, and the insert is *underlined and italic*. [b] For the resulting peptide sequence the insert is *underlined and italic*. [c] Constructed from partial library approach, selected sequence indicated.

Table 2. Primer Sets for Osteoblast Cell Markers

name		sequence 5−3	length (bp)
collagen pro-α-1 type I chain	COL1-Fw	5′GGAGAGAGCATGACCGATGGA3′	101
	COL1-Re	5′GGTGGACATTAGGCGAGGAA3′	
osteopontin	OP-Fw	5′TGAAAGTGACTGATTCTGGCA	375
	OP-Re	5′GGACGATTGGAGTGAAAGTGT	
alkaline phosphatase	ALP-Fw	5′CCAGCAGGTTTCTCTCTTGG3′	239
	ALP-Re	5′ CTGGGAGTCTCATCCTGAGC3′	
osteocalcin	OCN-Fw	5′CTCACTCTGCTGGCCCTG3′	257
	OCN-Re	5′CCGTAGATGCGTTTGTAGGC3′	
dentin matrix protein 1	Dmp1-Fw	5′CCCAGAGGCACAGGCAAATA3′	211
	Dmp1-Re	5′TCCTCCCCACTGTCCTTCTT3′	
β-actin	BAT-Fw	5′GTCCCTCACCCTCCCAAAAG3′	266
	BAT-Re	5′GCTGCCTCAACACCTCAACCC3′	

(0−4.5 mM) in culture media, as described in the above cell culture conditions.

Immunostaining and Data Analysis. Cells were fixed in 3.7% formaldehyde solution for 15 min and then blocked with a solution of 0.3% Triton X-100 and 5% normal goat serum in 1× PBS for 30 min. To stain the cell cultures, primary antibodies for identifying cell markers and for M13 phage were incubated with the cells overnight at 4 °C. The primary antibodies used in this investigation were mouse anti-β-tubulin III antibody (1:400, Sigma Aldrich, St. Louis, MO), mouse monoclonal anticollagen Type I antibody (1:1000, Sigma), and rabbit anti-fd antibody (1:500, Sigma Aldrich, St. Louis, MO). Secondary goat Alexa flouro-chrome-conjugated antibodies (Molecular Probes, Eugene, OR) and actin phalloidin were used at a dilution of 1:250 to visualize the markers and incubated with the cells for 2 h at room temperature. A DAPI (Molecular Probes, Eugene, OR) solution in PBS was used as a nuclear counterstain for all samples. The fluorescence images were collected using an IX71 Fluorescence Microscope (Olympus, Tokyo, Japan) and analyzed using NIH ImageJ (NIH, http://rsb.info.nih.gov/ij/).

ALP Activity Assays. QuantiChrom Alkaline Phosphatase Assay Kit (DALP-250, BioAssay Systems, Hayward, CA) was used to detect ALP activity. This kit utilizes *p*-nitrophenyl phosphate that is hydrolyzed by ALP into a yellow product (maximal absorbance at 405 nm). The rate of the reaction is directly proportional to the enzyme activity. Activity was measured as described in the manufacturer's manual.

Quantitative Real-Time Polymerase Chain Reaction (qRT-PCR). Quantitative real-time polymerase chain reaction (qRT-PCR) was conducted on iQ5 Real Time PCR using total RNA extracted and individual primer sets for collagen type I (COL1), osteopontin (OP), alkaline phosphatase (ALP), osteocalcin (OCN), dentin matrix acidic phosphoprotein 1 (Dmp1), and β-actin (BAT; see Table 2) with iScript One-Step RT-PCR Kit (Bio-Rad, Hercules, CA). Data for all genes were characterized by the cycle threshold (Ct), defined as the fractional number of cycles at which the reporter fluorescent emission reached a fixed threshold level in the exponential region of the amplification plot. Melting curves were plotted at the end of each experiment, with all products demonstrating one predominant peak. Relative expression was calculated by the ΔC_t method (where C_t is the threshold cycle) and values normalized to BAT.

ARS Assays (Alizarin Red S-Based Calcification Assay). Calcification was quantified by Alizarin Red S staining and organic extraction. Cells were washed three times with 150 mM NaCl and fixed with 70% ethanol for 30 min at room temperature. The fixed cells were then washed three times with 25% ethanol followed by H_2O. After addition of Alizarin Red S (0.5%) pH 5.0 (1 mL/well), the cells were incubated for 10 min at room temperature, before the Alizarin Red solution was aspirated. The wells were then washed four times with 1× PBS (pH 7.4) to remove unbound Alizarin Red, and the deposited Alizarin-Ca^{2+} complexes were extracted by the addition of 1−2 mL of 10% CPC. This extract was diluted in a 1:10 ratio, and then measured at an absorbance value of 570 nm with an ELISA reader. The absorbance values (A_{570}) were normalized to total cellular protein, which was determined by the Bradford assay.[59]

3. RESULTS AND DISCUSSIONS

We constructed major coat engineered phage with collagen-derived bone cell stimulating peptides motif (DGEA) and their controls, DGDA- and EGEA-peptides. The M13 phage is a bacterial virus composed of a single-stranded DNA encapsulated by various major and minor coat proteins in a nanofibrous shape (880 × 6.6 nm). Through the insertion of a desired gene, we can construct a nanofiber-like phage to express 2700 copies of the

dx.doi.org/10.1021/bm1013475 |*Biomacromolecules* XXXX, XXX, 000–000

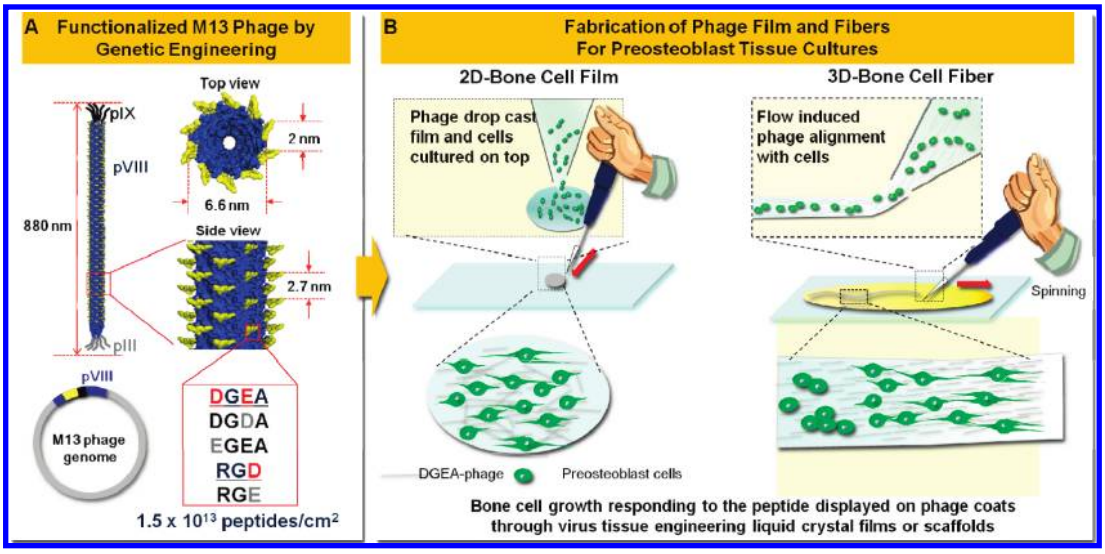

Figure 1. Schematic diagram of phage engineering and phage-based tissue matrix fabrication. (A) DGEA-engineered M13 structures by genetic engineering. (B) Schematic illustration of the overall strategy for fabricating two-dimensional drop cast film and three-dimensional aligned phage tissue matrices.

target peptides uniformly on the major coat surface with 2 and 2.7 nm spacing laterally and axially, respectively (Figure 1A).[60,61] DGEA (Asp-Gly-Glu-Ala) is a collagen type I motif and has exhibited specific binding for osteoblasts via $\alpha 2\beta 1$ integrin.[30,32] DGDA- and EGEA-peptides were chosen as controls for DGEA as they have the same charge value as DGEA. In addition, we use previously developed integrin-binding peptide engineered phage, RGD-phage, and its control phage, RGE-phage as another control (Table 1). RGD (Arg-Gly-Asp) is a well-characterized integrin-binding peptide that induces focal adhesion, helps cells to migrate, proliferate, and determines cellular morphology and fate.[29] RGE (Arg-Gly-Glu) is a nonadherent control peptide but has the same charge value as RGD. Previously, we constructed RGD-engineered phage (RGD-phage) on the major coat protein of M13 and demonstrated that RGD-phage can induce specific focal adhesion to stimulate cells to migrate, proliferate, and grow through the self-aligned nanofibrous tissue networks.[51−53] To evaluate the cell−ligand interactions on the nanofibrous matrices, we investigated the initial attachment, proliferation and osteoblast protein expression of MC3T3 cells on the M13 expressing various modified peptides using previously established 2D self-aligned phage films and 3D phage fibers (Figures 1B and S1).[51−53]

We first characterized the effect of the DGEA-peptide on the MC3T3 on 2D phage drop cast films (Figure 2A). We cultured MC3T3 directly on top of the drop-cast phage substrates to evaluate the specificity of biochemical ligands expressed on the phage, including DGEA-, RGD-, RGE-, and wildtype (no modification)-phages. The cell morphology on each phage film was observed and analyzed at 3, 6, and 12 h after cell seeding. Figure 2A consists of fluorescent micrographs showing preosteoblasts fixed at 12 h after seeding. We could observe pronounced outgrowth of the preosteoblast on DGEA-phage matrices. The cells are spread very well throughout the samples on the DGEA-phage matrices. Cells on RGD-phage matrices also exhibited a well-spread morphology, but their cell sizes were much smaller than those of DGEA-phage matrices. In contrast, on top of RGE- and wildtype-phage matrices, the cell number and their areas were reduced with increase in culture time (Figure 2B and 2C). Time-dependent quantitative measurement of the cell area at 3, 6, and 12 h after cell seeding on the phage coated surfaces indicates that cells start to spread at 3 h and increase their area attached onto surfaces during culture in a chemical ligand dependent manner (Figure 2B). Although integrin-binding peptide (RGD) has been known to play a critical role in cell spreading through focal adhesion over RGE-peptide, little difference in cell spreading was observed among RGD-, RGE- and wildtype-phage substrates when compared with those of the DGEA substrates. The DGEA-phage matrices exhibited similar cell spreading to that of the RGD-phage matrices, while the cells on DGEA-phages were more well spread and exhibited the largest cell areas as compared to those on RGD-phages, even at 3 h and reached maximum point at 12 h. The observed spreading morphologies and cell areas indicate that the DGEA-peptide ligand plays a significant role in bone cell morphological controls.

Using the WST1 assay, we also characterized MC3T3 cell viability and proliferation in 2D drop cast phage matrices. We cultured the MC3T3 on top of DGEA-, RGD-, RGE- and wildtype- phage matrices and quantified the proliferation rate by measuring the absorbance of the system at 420−480 nm (A_{max} 450 nm) in a multiwell plate reader on 1, 3, and 5 days after cell seeding. As shown in Figure 2C, MC3T3 cells on DGEA-phage matrices showed the highest metabolic activities which are very similar to RGD-phage matrices in their proliferation rate and growth. In contrast, RGE and wildtype phage matrices showed lower metabolic activities than those of DGEA- and RGD-phage matrices. DGEA-phage matrix effects are comparable with those of RGD- phage matrices. The similar proliferation rate between RGD- and DGEA-phage implies that DGEA-phage matrices may have similar roles in stimulating preosteoblasts to proliferate as RGD-peptide matrices do.

This DGEA-peptide specific outgrown morphology of preosteoblasts from the 2D cultures phage matrices was also observed in 3D cultures (Figure 2D). We first fabricated 3D aligned phage fiber matrices using our previously reported methods.[51] In short, suspensions of DGEA- and RGD-phage were prepared and mixed with 1 μL of cells at a density of 2×10^6 cells/mL and the final concentration was set at ~15 mg/mL. At this concentration,

dx.doi.org/10.1021/bm1013475 |*Biomacromolecules* XXXX, XXX, 000–000

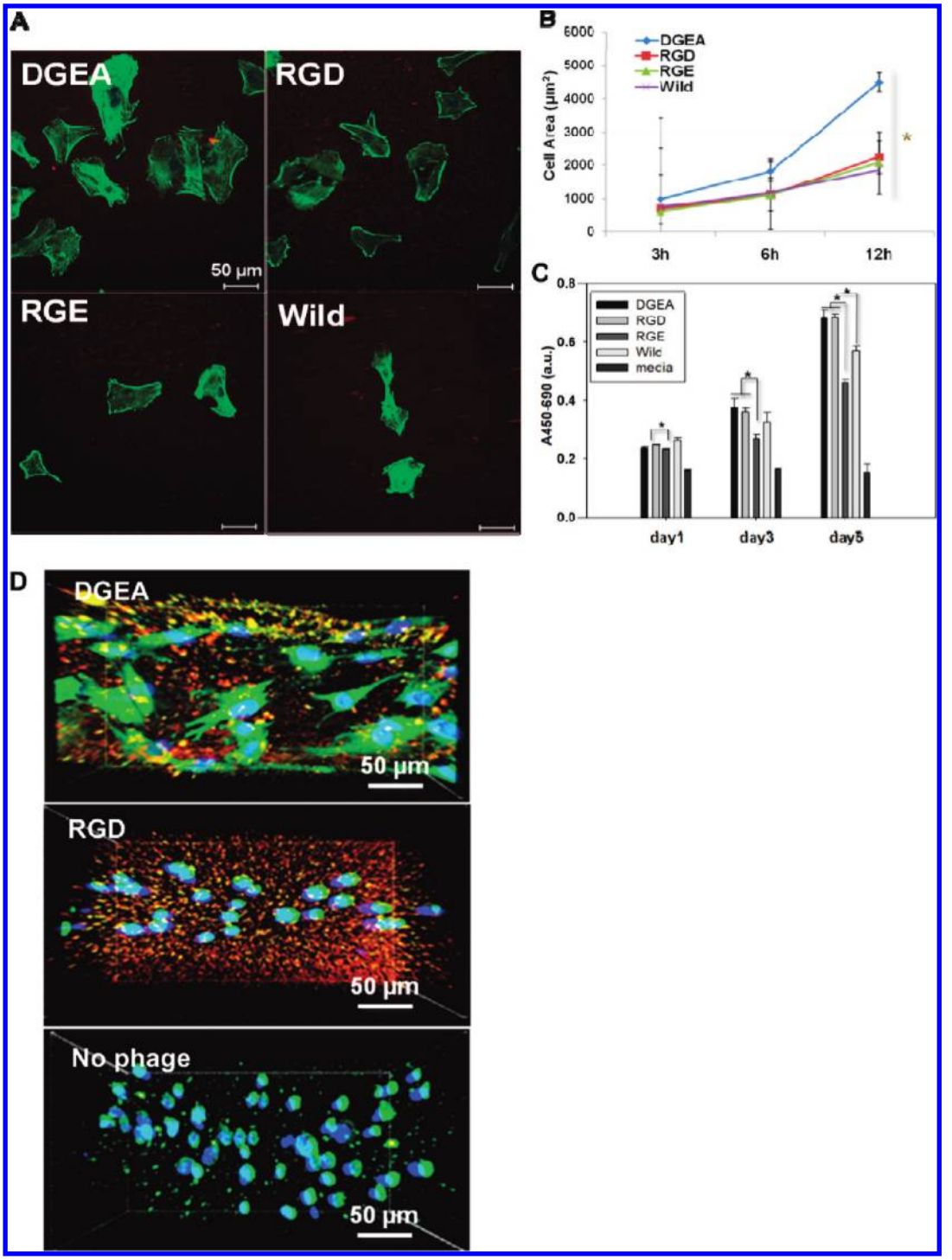

Figure 2. Outgrown morphology of preosteoblasts stimulated by DGEA-phage tissue matrices. (A) Fluorescent microscopy images of outgrown preosteoblasts after 12 h culture. The cells are stained by β-tubulin III (green), DAPI (blue), phage (red). (B) Quantification of the cell areas on phage film with different types of modification after 3, 6, and 12 h culture. Two to three fields of views were taken to analyze each images (cell $n = 3-14$ per one field of view, $^*p < 0.01$, ANOVA). (C) WST1 cell proliferation assays on different types of phages. WST1 assay result shows that cells on DGEA- and RGD-phages have a higher proliferation rate over those on RGE or wild phages ($^*p$-value < 0.05). (D) Confocal microscopy images of the outgrown preosteobasts at day 2 on 3D phage fiber with DGEA-, RGD- or no-phages mixed with 15% agarose gel. (DAPI (blue), β-tubulin III (green), phage (red), scale bar = 20 μm). Data are shown as means $\pm$ standard deviation (SD) of three independent samples ($^*p < 0.05$, ANOVA).

the phage formed the nematic phase liquid crystalline matrices where all phage particles were aligned in orientationally ordered structures. Ten μL of the cell and phage mixture was then manually injected directly into low melting temperature liquid agarose (1.5% w/v in PBS) and then the 3D fiber structure was solidified in agarose. The resulting agarose-templated phage-cell 3D aligned fiber-matrices formed a convenient 3D-cell culture system. Preosteoblasts on DGEA-phage 3D fiber matrices started

dx.doi.org/10.1021/bm1013475 |*Biomacromolecules* XXXX, XXX, 000–000

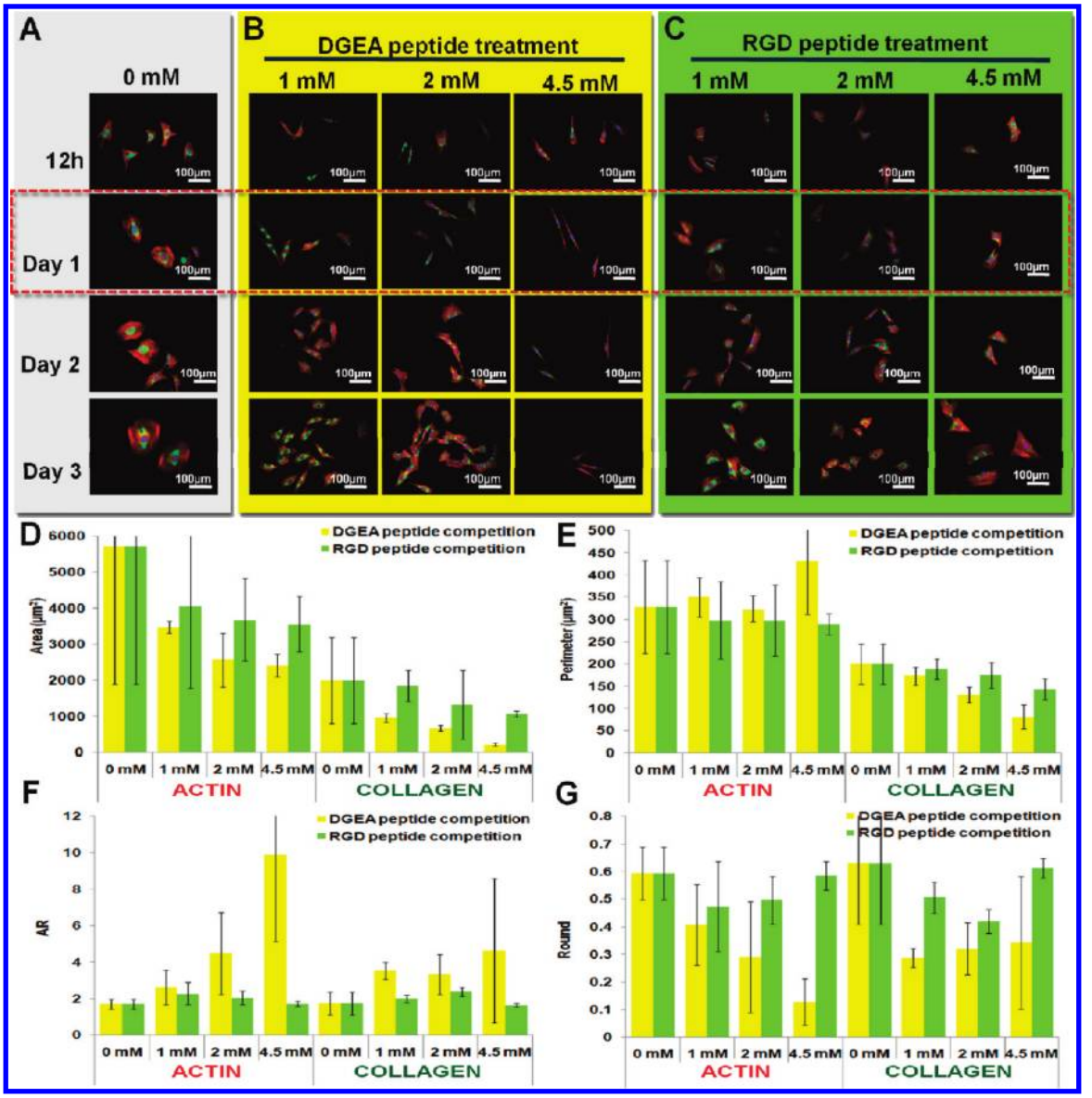

Figure 3. Competition assay with DGEA- and RGD-peptide against DGEA-phages. (A) Fluorescent microscopy images of preosteoblasts cultured on DGEA-phage film as a control. Preosteoblasts on the DGEA-phage matrices cultured with synthetic (B) DGEA- or (C) RGD-peptide treatment at different concentrations. Actin and collagen were stained phalloidin (red) and collagen type I antibody (green), respectively. The bar graph shows the quantification of actin and collagen (D) area, (E) perimeter, (F) AR, and (G) round in cells on DGEA-phage film in competition with DGEA- or RGD-peptides. Each experiment was performed in duplicates. Two to three fields of views were taken to analyze each images (D−G, cell $n = 3-5$ per one field of view, $p < 0.05$, ANOVA; DGEA vs RGD-peptides).

to spread very well along the phage fiber, as observed at day 1 (data not shown). All cells were stretched and spread well by day 2 (Figure 2D). However, cells on RGD-phage fiber or no-phage agarose gel fiber showed much less cell spreading by day 2 compared to those observed in DGEA-phage matrices. From proliferation assays in 2D phage matrices, RGD-peptide and DGEA-peptide showed similar attachment and proliferation rates during the five-day culture (as shown in Figure 2C). However, the preosteoblast cultured on the DGEA-phage matrices exhibited significantly more outgrown cell morphologies as compared to those of RGD-phage (Figure 2A,B). As mechanical stiffness is an important parameter on cellular growth processes, the observed outgrown morphologies from MC3T3 in 2D and 3D cell culture might be caused by the difference in mechanical stiffness between the 2D, 3D matrices and the agarose-template. However, the cellular morphologies from the control 3D RGD-phage matrices did not exhibit such cellular spreading. From these results, we could confirm that the DGEA-peptide plays a critical role in three-dimensional cell spreading.

We next investigated the specific DGEA-peptide effects on cell spreading using soluble DGEA-peptide competition assay. We first synthesized DGEA- and RGD-peptides using FMOC peptide synthesis approach. We then cultured MC3T3 on DGEA-phage coated culture slides (Lab-TekII chamber slides, Nalgen Nunc International, Naperville, IL) with 0, 1, 2, and 4.5 mM of DGEA- or RGD-peptide treatment in culture media. Cells were cultured and fixed at 12 h and days 1, 2, and 3, and actin filaments and collagen were fluorescently stained (Figure 3). As the concentration of soluble peptide increases, cell spreading decreases. Soluble DGEA-peptide treated preosteoblast morphologies showed

dx.doi.org/10.1021/bm1013475 |*Biomacromolecules* XXXX, XXX, 000–000

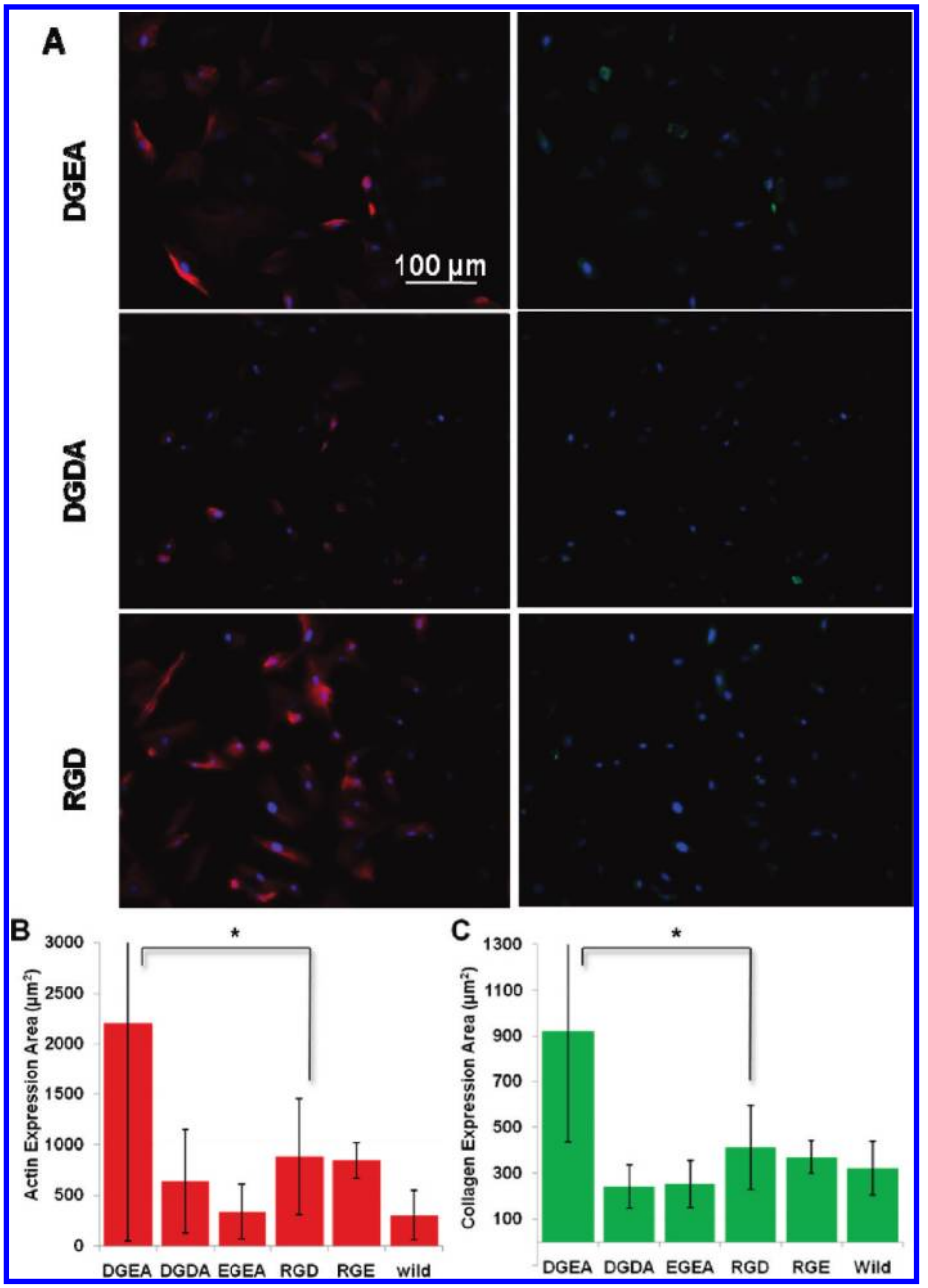

Figure 4. Outgrown preosteoblasts and relationship with actin and collagen expression on phage tissue matrices. (A) Fluorescent microscopy image of preosteoblasts on DGEA-, DGDA-, and RGD-phage matrices. Actin and collagen were stained phalloidin (red) and collagen type I antibody (green), respectively. (B, C) Quantification of actin and collagen shows that DGEA-phages induced much higher outgrown cellular morphologies and collagen expression over different types of phages. Each experiment was performed in duplicate (cell $n = 14-36$ per one field of view, $p < 0.01$, ANOVA).

that areas of actin filament and collagen expression decreased with increase in soluble DGEA-peptide concentration. Without competing peptide treatment, preosteoblasts exhibited increasing actin filaments and collagen expression with increase of culture time (Figure 3A). With DGEA-peptide competition treatment, the cells spread less (narrowly elongated cellular morphology) than those observed in RGD-peptide competition treatment (Figure 3B). In addition, when we cultured preosteoblasts for a longer time period, the preosteoblasts recovered their areas of actin and collagen expression when treated with a lower concentration range (lower than 2 mM of competing peptide solution). However, RGD-peptide treated cultures also recovered by increasing the areas of actin and collagen expression from the first day with increase of culture time and concentration of competing peptide, even up to 4.5 mM. Cells cultured on DGEA-phage showed higher actin filament and collagen expressions, which dramatically decrease when DGEA-peptide was added as a soluble competing ligand. This observation, that RGD-treatment caused the decreased expression of actin filaments and collagen, might originate from competition in adhesion forces provided by DGEA-peptide displayed on M13 phage (Figure 3C). Using the cell images at day1 (dotted red box in Figure 3C), we analyzed cell morphological parameters, including areas, perimeters, aspect ratio (AR), and roundness of regions where actin and collagen were expressed (Figure 3D−G). Area decreased with DGEA- and RGD-treatment in a dose-dependent manner but

dx.doi.org/10.1021/bm1013475 |*Biomacromolecules* XXXX, XXX, 000–000

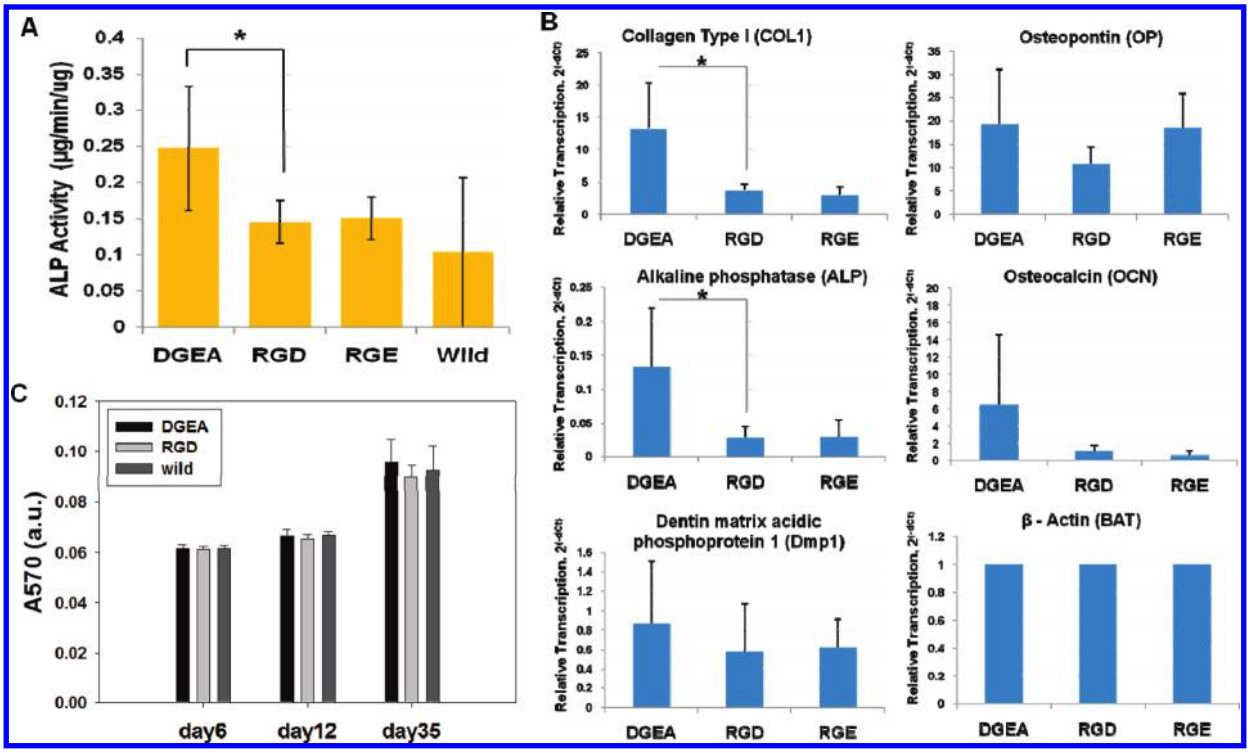

Figure 5. Bone cell function on DGEA-phages. (A) Alkaline phosphatase activity on DGEA-phages over RGD-, RGE-, and wild-phages. Data are shown as means ± standard deviation (SD) of three independent samples (*$p < 0.05$, ANOVA). (B) Quantification of osteogenic differentiation marker protein expression in preosteoblasts stimulated by DGEA-, RGD-, or RGE- phage using qRT-PCR. Alkaline phosphatase (ALP), collagen type I, osteopontin, osteocalcin, and dentin matrix acidic phosphoprotein I (DmpI) were quantified and normalized by β-actin was used as control gene. Data are shown as means ± standard deviation (SD) of five independent samples (*$p < 0.05$, ANOVA). RNAs extracted from cells cultured on DGEA-, RGD-, and RGE-phages (at 12 h culture) from each experiment were used. (C) Long time culture induces cell response to many other environmental factors, such as already fully secreted ECM, etc., so that MC3T3 cells were fully differentiated on all substrates. ARS data are shown as means ± standard deviation (SD) of MC3T3 calcification ($n = 4$). MC3T3 cells on all substrates formed calcified ECM (days 6, 12, and 35).

was more strongly affected with DGEA-peptide treatment. While the area decreased in DGEA-peptide competition treatment, cell perimeter increased in 4.5 mM DGEA-peptide competition treatment. Decreased area and increased perimeters can be interpreted as a result of a narrowed/shrunken but very elongated morphology. Higher aspect ratio and lower roundness also validates that point. The highest concentration, 4.5 mM of DGEA-peptide competition treatment, showed highly shrunken and narrowed cells in DGEA-peptide competition versus DGEA displayed on M13 phages and could not be recovered with increase of culture time. Therefore, we may conclude that wider cell spreading by actin filaments and collagen expression on DGEA-phages originates from the effect of the high density DGEA-peptides on phage major coat proteins.

Based on our observation in the 2D and 3D preosteoblast culture, the pronounced cellular outgrowth morphologies are highly dependent on the presence of the DGEA-motif. In addition, it is previously known that type I collagen-induced osteoblast differentiation is mediated by collagen−$\alpha 2\beta 1$ integrin interaction.[30] Therefore, we hypothesized that DGEA-specific morphology could be linked to initial differentiation, which will be correlated to osteoblast cell marker expressions. Therefore, we further investigated the relationship between cell spreading and osteoblast cell marker expression in the MC3T3 on nanofibrous DGEA−phage matrices and its controls (DGDA-, EGEA-, RGD-, RGE-, and wild-phages). We first cultured the MC3T3 cells on the top of the drop-cast films on the DGEA-phage and control matrices and immuno-fluorescently stained the actin filaments and collagen type I, an osteoblastic cell marker. We then characterized the cellular morphology of the MC3T3 in terms of actin and collagen expression (Figure 4) depending on the chemical ligands. We labeled actin and collagen type I using phalloidin and collagen type I antibody respectively (Figure 4 and Figure S2). We observed that all samples exhibited actin filaments and collagen expressions in different amounts depending on the peptide sequences of the phage. The wide-spreading morphological response of osteoblast cells to DGEA can be seen in the well-spread and stretched actin filaments staining and wider collagen expression of MC3T3 cells on DGEA-phages. DGEA- and RGD-phage matrices exhibited similar cellular density and attachments. Quantified actin filament expression and collagen expression areas at 12 h after seeding showed that the cell spreading on the DGEA-phages was supported by actin filament expression (Figure 4B), which is, in turn, correlated with collagen expression (Figure 4C). These observations are well matched with the cell area measurement that we previously characterized (DGEA > RGD > RGE > Wild), as shown in Figure 2B. DGDA- and EGEA-phages did not show these specific responses, which confirmed that it is DGEA-peptide sequence specific. Therefore, DGEA-phage matrices exhibited pronounced expression of actin and collagen type I proteins in a DGEA-specific biochemically dependent manner.

We further characterized the early osteogenic responses by quantifying the marker protein activity and its mRNA expression. By measuring alkaline phosphatase (ALP) activity, one of the osteogenic differentiation markers, we characterized the early responses to the DGEA-peptides. Preosteoblasts cultured on top

of DGEA-phage matrices (day 1) showed ~70% more ALP activity as compared to those on RGD- phage matrices (Figure 5A). These initial osteogenic responses were also confirmed by the mRNA quantification of differentiation marker proteins in the preosteoblasts stimulated by the DGEA-motif. We performed qRT-PCR and quantified the initial expression of five osteogenic protein markers on MC3T3 cells based on the engineered peptides on the phages: collagen type I (COL1), osteopontin (OP), alkaline phosphatase (ALP), osteocalcin (OCN), and dentin matrix acidic phosphoprotein 1 (Dmp1) with RNA extracted from MC3T3 at 12 h culture (Figure 5B). We used β-actin (BAT) as an endogenous protein control. We used the "relative quantification" method to validate the expression results.[62] Fully developed osteoblastic differentiation marker protein expression in preosteoblast normally takes over 2 weeks.[63,64] Using qRT-PCR, we could observe evidence of early stage osteogenic differentiation effects. Figure 5B shows the relative normalized RNA expression marker values compared to the β-actin RNA expression on DGEA-, RGD-, and RGE-matrices at 12 h after seeding with ascorbic acid treatment (Figure 5B, Table S1). All quantification showed that DGEA-phage exhibited the most pronounced expression of the osteogenic protein marker as compared to RGD- and RGE-controls. The preosteoblasts on DGEA-phages also show relatively up-regulated expressions on each osteogenic protein markers over those on RGD- or RGE- phages. Early responsive collagen type I and osteopontin showed comparably higher expression.

To investigate the effect of the DGEA-phage matrices on the preosteoblasts at a later stage, we characterized the response of osteogenic protein expressions and their functions using alizarin red staining (ARS) assays on days 6, 12, and 35 (Figure 5C). The ARS assay is an osteogenesis assay that shows how much calcium phosphate is deposited onto the mineralized tissue matrices. Through quantification of the calcium amount using alizarin staining, we could measure osteogenic activities resulting in calcification of calcium phosphates stimulated by the chemical signals from the engineered phages (DGEA, RGD, and wild-type). The ARS results showed that DGEA-peptides on the phage matrices have little effect on the later stages of differentiation of the osteoblast which was induced by ascorbic acid and melatonin. All cells exhibited similar calcification morphologies (data not shown) and the ARS reading on days 6, 12, and 35 exhibited very similar values (Figure 5C). Based on our initial and later stage characterization experiments, it is likely that mouse preosteoblasts are stimulated by phage matrices, expressing the DGEA peptide in the early stages of differentiation and respond by expressing actin and collagen type I, leading to an outgrown cell morphology. These outgrown cellular morphologies of the preosteoblasts were accompanied by the initial expression of early osteogenic differentiation markers that we could observe from mRNA expression (Figure 5B). However, we postulate that, with prolonged culture periods, the cells began to secrete more ECM proteins, which diluted the effects of the ligands expressed on our engineered phage. Therefore, we could not observe significant morphological changes in the later stages of differentiation.

In this study, we observed outgrown cellular morphology and pronounced initial osteogenic protein expression of the bone progenitor cells (MC3T3) stimulated by the collagen-derived DGEA-peptide. DGEA-peptides adopt a specific role to stimulate expression of cytoskeleton proteins, such as actin filaments, and osteogenic proteins, such as collagen type I, osteopontin, alkaline phosphatase (ALP), osteocalcin, and dentin matrix acidic phosphoprotein I (DmpI), even at early stages (12 h to 1 day) of differentiation. Based on our observation, we propose that DGEA-peptides help the preosteoblasts to spread with a stretched morphological response to initial osteogenic differentiation inductions. These pronounced osteogenic protein expressions are correlated with the outgrown morphologies stimulated by the DGEA-phage matrices. In our approach, we also demonstrated that our genetically engineered phage could provide a convenient toolkit for investigating specific functions of biochemical ligands. Through the insertion of a desired gene, we can express a high density of biochemical ligands on nanofibrous phage surfaces (1.5×10^{13} ligands/cm^2). Through mutagenesis of the genome of the phage, we could construct target biochemical ligands at a single amino acid level precision with little change in other parameters. After amplification, the resulting phage can be used to construct phage-based tissue matrices that present nanofibrous structures with similar presentation mode, density, and spacing. Therefore, the phage-based tissue matrix system is an important resource for investigating many other biochemical cues in cell biology and stem cell engineering in a systematic manner.

4. CONCLUSIONS

We present a novel bottom-up approach employing phage technology to construct collagen-like nanofibrous-shaped phages that display bone−cell specific collagen-derived DGEA-peptides for controlling preosteoblast cellular growth processes. Our DGEA-engineered phage matrices can induce outgrown preosteoblast cell morphologies and stimulate osteogenic protein expression in the initial stages of osteogenic differentiation. This study shows a systemic approach of interpreting the peptide function embedded in phage-based matrices, which is essential for successfully developing advanced biomimetic and biocompatible materials for bone tissue engineering. Our results show further possibilities to develop advanced phage-based peptide display and their functional studies will aid in the development of functional biomaterials for regenerative medicine.

■ ASSOCIATED CONTENT

Supporting Information. AFM images of nanofiber-like M13 phages tissue matrices. MC3T3 cells cultured on 2D- or 3D-phage matrices. Osteoblastic markers RNA expression values. This material is available free of charge via the Internet at http://pubs.acs.org.

■ AUTHOR INFORMATION

Corresponding Author

*Tel.: +1-510-486-4628. Fax: +1-510-486-6488. E-mail: leesw@berkeley.edu.

■ ACKNOWLEDGMENT

This work was supported by the Hellman Family Faculty Fund (S.-W.L.), start-up funds from the Berkeley Nanoscience and Nanoengineering Institute at the University of California, Berkeley (S.-W.L.), and the Laboratory Directed Research and Development fund from the Lawrence Berkeley National Laboratory.

■ REFERENCES

(1) Bearinger, J. P.; Terrettaz, S.; Michel, R.; Tirelli, N.; Vogel, H.; Textor, M.; Hubbell, J. A. *Nat. Mater.* **2003**, *2* (4), 259–264.

(2) Falconnet, D.; Csucs, G.; Michelle Grandin, H.; Textor, M. *Biomaterials* **2006**, *27* (16), 3044–3063.
(3) Lussi, J. W.; Falconnet, D.; Hubbell, J. A.; Textor, M.; Csucs, G. *Biomaterials* **2006**, *27* (12), 2534–2541.
(4) Lussi, J. W.; Csucs, G.; Textor, M.; Hubbell, J. A.; Danuser, G. *Mol. Biol. Cell* **2002**, *13*, 1898.
(5) Qin, D.; Xia, Y. N.; Whitesides, G. M. *Nat. Protoc.* **2010**, *5* (3), 491–502.
(6) Stevens, M. M.; Mayer, M.; Anderson, D. G.; Weibel, D. B.; Whitesides, G. M.; Langer, R. *Biomaterials* **2005**, *26* (36), 7636–7641.
(7) Xia, Y.; Whitesides, G. M. *Annu. Rev. Mater. Sci.* **1998**, *28* (1), 153–184.
(8) Tang, Z.; Wang, Y.; Podsiadlo, P.; Kotov, N. A. *Adv. Mater.* **2006**, *18* (24), 3203–3224.
(9) Ren, K.; Crouzier, T.; Roy, C.; Picart, C. *Adv. Funct. Mater.* **2008**, *18* (9), 1378–1389.
(10) Bettinger, C. J.; Langer, R.; Borenstein, J. T. *Angew. Chem., Int. Ed.* **2009**, *48* (30), 5406–5415.
(11) de Mel, A.; Jell, G.; Stevens, M. M.; Seifalian, A. M. *Biomacromolecules* **2008**, *9* (11), 2969–2979.
(12) Anderson, J. M.; Kushwaha, M.; Tambralli, A.; Bellis, S. L.; Camata, R. P.; Jun, H.-W. *Biomacromolecules* **2009**, *10* (10), 2935–2944.
(13) Khew, S. T.; Tong, Y. W. *Biomacromolecules* **2007**, *8* (10), 3153–3161.
(14) Huber, A. B.; Kolodkin, A. L.; Ginty, D. D.; Cloutier, J. F. *Annu. Rev. Neurosci.* **2003**, *26*, 509–563.
(15) Milner, R.; Campbell, I. L. *J. Neurosci. Res.* **2002**, *69* (3), 286–91.
(16) Rutka, J. T.; Apodaca, G.; Stern, R.; Rosenblum, M. *J. Neurosurg.* **1988**, *69* (2), 155–170.
(17) Oster, S. F.; Deiner, A.; Birgbauer, E.; Sretavan, D. W. *Semin. Cell Dev. Biol.* **2004**, *15* (1), 125–136.
(18) Gumbiner, B. M. *Cell* **1996**, *84* (3), 345–357.
(19) Gospodarowicz, D.; Delgado, D.; Vlodavsky, I. *Proc. Natl. Acad. Sci. U.S.A.* **1980**, *77* (7), 4094–4098.
(20) Hynes, R. O. *Cell* **1992**, *69* (1), 11–25.
(21) Pamula, E.; De Cupere, V.; Dufrêne, Y. F.; Rouxhet, P. G. *J. Colloid Interface Sci.* **2004**, *271* (1), 80–91.
(22) Bozec, L.; van der Heijden, G.; Horton, M. *Biophys. J.* **2007**, *92* (1), 70–75.
(23) Johansson, J. Å.; Halthur, T.; Herranen, M.; Söderberg, L.; Elofsson, U.; Hilborn, J. *Biomacromolecules* **2005**, *6* (3), 1353–1359.
(24) Alexander, N. R.; Branch, K. M.; Parekh, A.; Clark, E. S.; Iwueke, I. C.; Guelcher, S. A.; Weaver, A. M. *Curr. Biol.* **2008**, *18*, 1295–1299.
(25) Roy, K.; Mao, H.-Q.; Lim, S. H.; Zhang, S.; Christopherson, G.; Kam, K.; Fischer, S. *Biomaterials as Stem Cell Niche*; Springer: Berlin Heidelberg, 2010; Vol. 2, pp 89−118.
(26) Ruoslahti, E. *Ann. Rev. Cell Dev. Biol.* **1996**, *12*, 697–715.
(27) Discher, D. E.; Mooney, D. J.; Zandstra, P. W. *Science* **2009**, *324* (5935), 1673–1677.
(28) Hynes, R. O. *Trends Cell Biol.* **1999**, *9* (12), M33–M37.
(29) Pierschbacher, M. D.; Ruoslahti, E. *Nature* **1984**, *309* (5963), 30–3.
(30) Mizuno, M.; Fujisawa, R.; Kuboki, Y. *J. Cell. Physiol.* **2000**, *184* (2), 207–213.
(31) Tashiro, K.; Sephel, G. C.; Weeks, B.; Sasaki, M.; Martin, G. R.; Kleinman, H. K.; Yamada, Y. *J. Biol. Chem.* **1989**, *264* (27), 16174–16182.
(32) Staatz, W. D.; Fok, K. F.; Zutter, M. M.; Adams, S. P.; Rodriguez, B. A.; Santoro, S. A. *J. Biol. Chem.* **1991**, *266* (12), 7363–7367.
(33) Taylor, P. M.; Allen, S. P.; Dreger, S. A.; Yacoub, M. H. *J. Heart Valve Dis.* **2002**, *11* (3), 298–306.
(34) Daamen, W. F.; van Moerkerk, H. T. B.; Hafmans, T.; Buttafoco, L.; Poot, A. A.; Veerkamp, J. H.; van Kuppevelt, T. H. *Biomaterials* **2003**, *24* (22), 4001–4009.
(35) Nakanishi, Y.; Chen, G.; Komuro, H.; Ushida, T.; Kaneko, S.; Tateishi, T.; Kaneko, M. *J. Pediatr. Surg.* **2003**, *38* (12), 1781–1784.
(36) Barrère, F.; Mahmood, T. A.; de Groot, K.; van Blitterswijk, C. A. *Mater. Sci. Eng.* **2008**, *59* (1−6), 38–71.
(37) Douglas, T.; Young, M. *Nature* **1998**, *393* (6681), 152–155.
(38) Lee, S. W.; Mao, C. B.; Flynn, C. E.; Belcher, A. M. *Science* **2002**, *296* (5569), 892–895.
(39) Naik, R. R.; Stringer, S. J.; Agarwal, G.; Jones, S. E.; Stone, M. O. *Nat. Mater.* **2002**, *1* (3), 169–172.
(40) Mao, C. B.; Solis, D. J.; Reiss, B. D.; Kottmann, S. T.; Sweeney, R. Y.; Hayhurst, A.; Georgiou, G.; Iverson, B.; Belcher, A. M. *Science* **2004**, *303* (5655), 213–217.
(41) Merzlyak, A.; Lee, S. W. *Curr. Opin. Chem. Biol* **2006**, *10* (3), 246–252.
(42) Nam, K. T.; Kim, D. W.; Yoo, P. J.; Chiang, C. Y.; Meethong, N.; Hammond, P. T.; Chiang, Y. M.; Belcher, A. M. *Science* **2006**, *312* (5775), 885–888.
(43) Du, B.; Han, H.; Wang, Z.; Kuang, L.; Wang, L.; Yu, L.; Wu, M.; Zhou, Z.; Qian, M. *Mol. Cancer Res.* **2010**, *8* (2), 135–144.
(44) Bar, H.; Yacoby, I.; Benhar, I. *BMC Biotechnol.* **2008**, *8* (1), 37.
(45) Li, K.; Chen, Y.; Li, S.; Nguyen, H. G.; Niu, Z.; You, S.; Mello, C. M.; Lu, X.; Wang, Q. *Bioconjugate Chem.* **2010**, *21* (7), 1369–1377.
(46) Frenkel, D.; Solomon, B. *Proc. Natl. Acad. Sci. U.S.A.* **2002**, *99* (8), 5675–9.
(47) Kreutzberg, G. W. *Trends Neurosci.* **1996**, *19* (8), 312–318.
(48) Hart, S. L.; Knight, A. M.; Harbottle, R. P.; Mistry, A.; Hunger, H. D.; Cutler, D. F.; Williamson, R.; Coutelle, C. *J. Biol. Chem.* **1994**, *269* (17), 12468–12474.
(49) Ivanenkov, V. V.; Felici, F.; Menon, A. G. *Biochim. Biophys. Acta, Mol. Cell Res.* **1999**, *1448* (3), 450–462.
(50) Chung, W.-J.; Merzlyak, A.; Yoo, S. Y.; Lee, S.-W. *Langmuir* **2010**, *26* (12), 9885–9890.
(51) Merzlyak, A.; Indrakanti, S.; Lee, S.-W. *Nano Lett.* **2009**, *9* (2), 846–852.
(52) Chung, W.-J.; Merzlyak, A.; Lee, S.-W. *Soft Matter* **2010**, *6* (18), 4454–4459.
(53) Yoo, S. Y.; Chung, W. J.; Kim, T. H.; Le, M.; Lee, S. W. *Soft Matter* **2011**, *7* (2), 363–368.
(54) Bruckman, M. A.; Kaur, G.; Lee, L. A.; Xie, F.; Sepulveda, J.; Breitenkamp, R.; Zhang, X.; Joralemon, M.; Russell, T. P.; Emrick, T.; Wang, Q. *ChemBioChem* **2008**, *9* (4), 519–523.
(55) Chen, G.; Courey, A. J. *BioTechniques* **1999**, *26*, 814–816.
(56) Qi, D.; Scholthof, K. B. *J. Virol. Methods* **2008**, *149* (1), 85–90.
(57) Merzlyak, A.; Indrakanti, S.; Lee, S. W. *Nano Lett.* **2009**, *9* (2), 846–52.
(58) Sambrook, J.; Russell, D. W. *Molecular Cloning: A Laboratory Manual*, 3rd ed.; CSHL Press: New York, 2001.
(59) Bradford, M. M. *Anal. Biochem.* **1976**, *7* (72), 248–254.
(60) Smith, G. P.; Petrenko, V. A. *Chem. Rev.* **1997**, *97* (2), 391–410.
(61) Petrenko, V. A.; Smith, G. P.; Gong, X.; Quinn, T. *Protein Eng.* **1996**, *9* (9), 797–801.
(62) Cikos, S.; Bukovska, A.; Koppel, J. *BMC Mol. Biol.* **2007**, *8* (1), 113.
(63) Alves, R. D. A. M.; Eijken, M.; Swagemakers, S.; Chiba, H.; Titulaer, M. K.; Burgers, P. C.; Luider, T. M.; van Leeuwen, J. P. T. M. *J. Proteome Res.* **2010**, *9* (9), 4688–47000.
(64) Otsuka, E.; Yamaguchi, A.; Hirose, S.; Hagiwara, H. *Am. J. Physiol. Cell. Physiol.* **1999**, *277* (1), C132–138.